Design of a High-Performance Humanoid Dual Arm System with Inner Shoulder Joints

Samuel Rader, Lukas Kaul, Hennes Fischbach, Nikolaus Vahrenkamp and Tamim Asfour

***Abstract*— This paper presents the design of the KIT Dual Arm System, which consists of two high-performance, humanoid robot arms. Based on human arm kinematics, each arm has 8 degrees of freedom (DOF) including a clavicle joint of the inner shoulder. In comparison to classical 7 DOF robot arms, the incorporation of the clavicle joint results in a larger workspace and an increased dexterity in bimanual tasks. The arm structure is based on an exoskeleton design approach: Highly modular and highly integrated sensor-actuator-control units in each joint are linked by a hollow structure, which allows a stiff construction at low weight. Combined with its length of 1 m and a maximum payload of 11 kg at stretched configuration, the performance of the KIT Arm is comparable to state-of-the art industrial robot arms. Thereby, it combines the strengths of humanoid and industrial robot arms.**

I. INTRODUCTION AND RELATED WORK

Physical human-robot interaction is becoming increasingly important, posing growing requirements for robot arms. Robot arms have to be strong while having a human appearance, precise while having a high payload-to-weight ratio and robust while having human kinematics. Additionally, they have to be safe. Today, most robot arms can be separated in two categories: industrial and humanoid robot arms.

Humanoid robots, which are mostly developed in scientific facilities, have a human appearance. Their human-like kinematics simplifies their application in human environments and the usage of human tools. Examples for lightweight arms with a humanoid appearance can be found in the humanoid robots HRP-2 [1], HRP-4C [2], ARMAR-III [3] and ARMAR-4 [4]. While most humanoid robot arms have 6 ([1][2][5]) or 7 degrees of freedom (DOF)[3][6][7], the arms of ARMAR-4 have 8 DOF each, reproducing a clavicle joint of the inner shoulder. Although this additional inner shoulder joint is beneficial for dual arm manipulation, it is only realized in few other robots, including the humanoid H6 [6] with two 7 DOF arms, or in complex shoulder prototypes [8]. The practical usage of humanoid robot arms is often limited due to imprecision, weakness or lack of robustness. Notable exceptions are the humanoid robots WALK-MAN [7] and ATLAS [5], which have robust high-performance arms. However, they are based on less humanoid kinematics: Neither WALK-MAN's wrist joints nor its shoulder joints intersect in a single point, and the arms of ATLAS have only 6 DOF.

The authors are with the High Performance Humanoid Technologies Lab, Institute for Anthropomatics and Robotics, Karlsruhe Institute of Technology (KIT), Germany, {rader, lukas.kaul, vahrenkamp, asfour}@kit.edu

The research leading to these results has received funding from the European Union's Horizon 2020 Research and Innovation programme under grant agreement No 643950 (SecondHands).

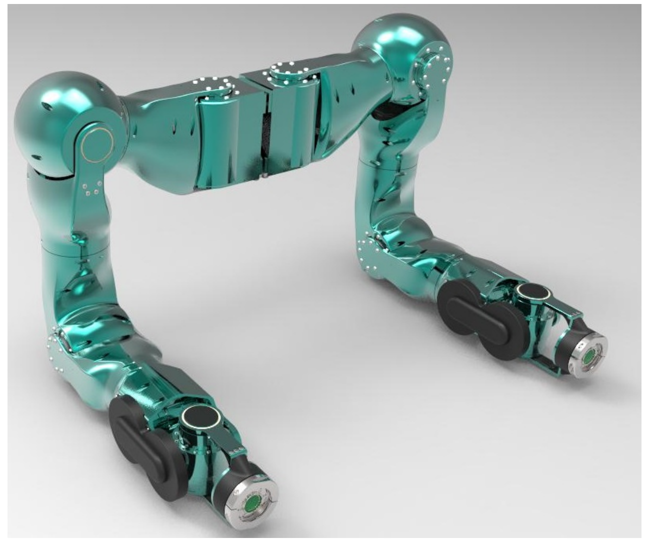

Fig. 1. KIT Dual Arm System (rendering)

A robust high-performance design with a large workspace is typical for industrial robot arms, such as the KUKA KR series [9]. These 6 DOF robot arms are frequently used in industrial manufacturing processes for pick-and-place tasks. The UR series by UNIVERSAL ROBOTS [10] combines these characteristics with a force sensing feature that allows for safe collaboration with humans. Using offsets between the axis of the upper arm, forearm and wrist, their kinematics are not anthropomorphic. A disadvantage of arms with 6 DOF is the lack of kinematic redundancy for a given 6D end-effector pose. Since obstacles, such as a second arm or a human, may limit the workspace, redundancy can be useful to resolve such situations. This is why in recent years, dual arm systems with 7 DOF arms have been developed. They can execute tasks such as loading, packing and material handling. Examples fur industrial two-arm systems are YuMi [11], BAXTER [12] and the MOTOMAN SDA series [13]. However, the maximum payload of BAXTER (2.2 kg) and YuMi (0.5 kg) is limited compared to most industrial arms, whereas the MOTOMAN SDA-series' usability for mobile setups as humanoid robots is limited due to the massive weight (110-380 kg).

Examples for robot arms that combine the advantages of industrial and humanoid robot arms are the KUKA 7 DOF lightweight arms [9]. They are based on the DLR LWR III [14][15], which is also used in a dual arm system as part of DLR's humanoid robot JUSTIN [16]. The DLR/KUKA lightweight arms combine humanoid kinematics with a high payload-to-weight ratio of up to 1.0, high precision, a robust modular design and compliance. Recently, FRANKA EMIKA [17] has been released as the next generation of lightweight arms.

This paper presents the KIT Dual Arm System, which consists of two high-performance, humanoid robot arms with 8 DOF each (Fig. 1). It combines human-like kinematics for humanoid robots with the strengths of industrial robot arms in a robust, modular design with a large bimanual workspace and a maximum payload of 11 kg. We argue that arms with 8 instead of 7 DOF are better suited for dual arm manipulation and we support this argument with a workspace analysis of the presented design.

The paper is organized as follows: Section II presents the characteristic data of the KIT Arm with a focus on its special human kinematics due to the realization of a clavicle joint of the human inner shoulder. This includes a detailed comparison with commercially available robot arms. In Section III, we describe the modular exoskeleton design approach we use for the KIT Arm that is currently being built. This is followed by a reachability and manipulability analysis of the arm in Section IV, showing the benefits of the clavicle joint for dual arm manipulation. Finally, Section V summarizes the results and concludes the paper.

II. KINEMATICS AND CHARACTERISTIC DATA

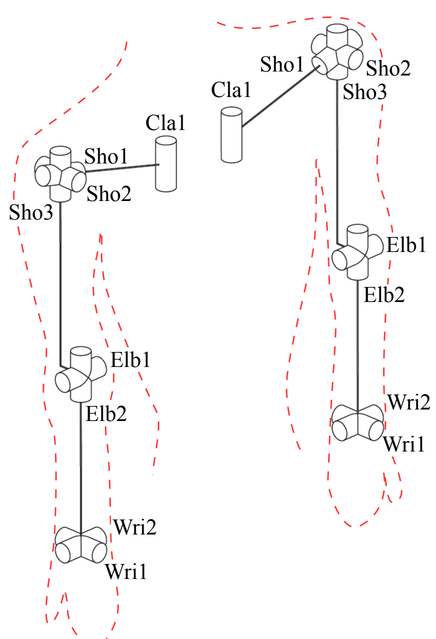

Fig. 2. Kinematic structure of the KIT Dual Arm System (front view)

A. Joint Configuration

The KIT Dual Arm System is a two arm system which consists of two identical robot arms, each of them having 8 DOF (see Fig. 2 and Table I). As depicted in Fig. 2, the joint *Cla1* is reproducing a clavicle joint of the human inner shoulder. It is followed by the three shoulder joints *Sho1-3*, which intersect in one point in order to emulate a spherical joint. The elbow consists of two intersecting joints (*Elb1, Elb2*). The joint axis of *Elb2* is intersecting with the two wrist joints *Wri1, Wri2* building a second spherical joint. Based on geometric conditions of the human body, we increased the flexion angle of the elbow joint *Elb1* by introducing a certain displacement between the upper arm and the forearm.

Joint	θ [°]	α[°]	a [mm]	d [mm]
Cla1	θ_1	75	0	0
Sho1	$-90+\theta_2$	90	0	300
Sho2	$75+\theta_3$	90	0	0
Sho3	$-90+\theta_4$	90	-55	409
Elb1	$180+\theta_5$	90	0	0
Elb2	$90+\theta_6$	90	0	364
Wri1	$90+\theta_7$	90	0	0
Wri2	θ_8	0	(227)	0

TABLE I

DENAVIT-HARTENBERG PARAMETERS OF A SINGLE KIT ARM (LEFT)

The kinematic structure and the decision to reproduce a clavicle joint of the human inner shoulder are inspired by [18], which proposes a model of the human arm kinematics with 9 DOF arm, including two clavicle joints of the inner shoulder. Based on our experience with ARMAR-4 [4] and workspace analysis, we decide to realize an 8 DOF arm, which includes one of the two clavicle joints. This provides a dexterous arm construction that supports bimanual tasks. As described in Section I, robot arms usually have only 6 or 7 DOF. A visualization of the kinematic structure of the KIT Dual Arm System with a focus on each joint's range of motion is presented in the video attachment.

B. Arm Proportions

Our aim is to develop a dual arm system for physical human-robot interaction that is able to assist humans in natural working environments such as a warehouse or a kitchen. As the arm is considered to fulfill different tasks as picking up objects from the floor as well from a high shelf, we seek a maximum range and workspace, especially, if no additional high adjustment is foreseen. However, the maximum length is limited through the ability of the arm to work in human environments. As compromise, we target an arm length of 1000 mm from the spherical joint of the shoulder to the tool center point (TCP).

Distances between	Human Length Large Operator ISO3411[19] [mm]	Scaled Length [mm]	Realized Length [mm]
Shoulder - Elbow	303	409	409
Elbow - Wrist	270	364	364
Wrist - Grip axis	137	185	(227)
Shoulder - Grip axis	710	958	(1000)

TABLE II

SCALED ARM DIMENSIONS

As end-effector, we foresee a humanoid hand. Based on concepts for the planned hand, we are assuming a distance of 227 mm between the wrist joint and the TCP. As we target human proportions, the distances between the joint axes Shoulder-Elbow and Elbow-Wrist are determined by scaling anthropometric data of human dimensions. ISO 3411 provides detailed information about physical dimensions of human machine operators, including the distances between the arm joints [19]. Based on the data of tall people, the 95th percentile (Table II, 2nd column), and a target length of 773 mm (1000 mm - 227 mm) between the shoulder and the wrist, we obtain a scaled distance of 409 mm between the shoulder and the elbow and a scaled distance of 364 mm between the elbow and the wrist (Table II, 3rd & 4th column). Assuming that the TCP lies in the grip axis and using the same scale factor, the distance between the wrist and the grip axis should be 185 mm and therefore a little bit smaller than the proposed distance of 227 mm (Table II, 3rd & 4th column). However, we foresee various end-effectors, whereby varying distances between the wrist and the TCP can be realized.

C. Range and Workspace

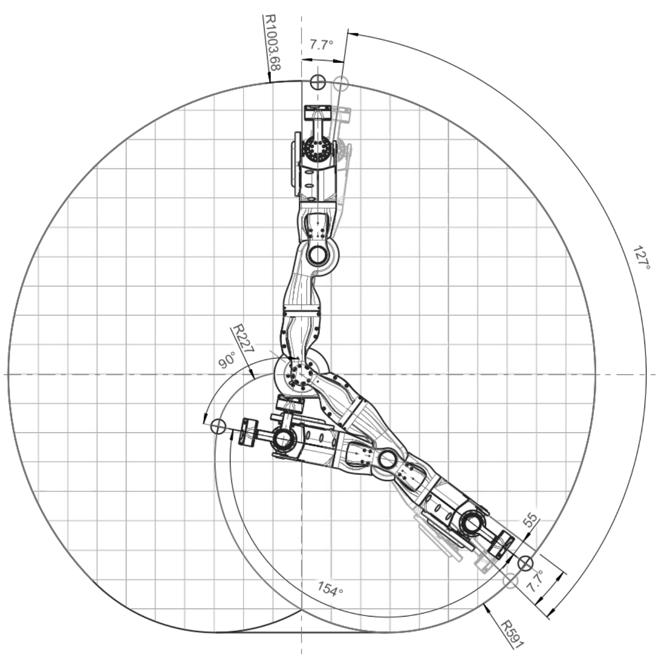

Fig. 3. Workspace of Sho1 and subsequent joints (sectional view)

Considering the range increase through the displacement between the forearm and the upper arm (55 mm), the maximal distance between the spherical shoulder joint and the TCP is increased from 1000 mm to approx. 1004 mm (at an *Elb1* angle of approx. 7.7°). But the arm range is not only given by the distance between the spherical shoulder joint (*Sho1-3*) and the TCP. Through the realization of the clavicle joint *Cla1*, the distance between the clavicle joint and the spherical shoulder joint (300 mm) must be added. This results in a range of approx. 1304 mm.

Fig. 3 presents the workspace of a single KIT Arm starting out from the *Sho2* joint axis. The arm range leads to a circle sector with a radius of 1004 mm. The joint limits of *Sho2* (see Table IV) are limiting this sector to 127°(202°-75°) plus 7.7° (displacement) from the *Sho1* axis. This is followed by smaller circle sectors around the *Elb1* joint axis (154°) and the *Wri2* axis (90°). Since the *Sho1* joint axis has no joint limits, this results in a rotation body with a volume of 4.2 m^3. This is the workspace without clavicle joint. For determining the workspace of the whole arm, the volume has to be rotated around the *Cla1* axis (+/-82°), which results in a significantly bigger workspace of 6.6 m^3.

Since many robot arms offer the possibility of changeable end-effectors, the arm range can also be described by giving the maximum distance between the first joint(s) of the shoulder and the wrist joint or the end effector flange. Table III compares the 8 DOF KIT Arm and a 7 DOF version (without clavicle joint) for different arm range definitions together with the resulting workspace. For every definition, the workspace is nearly doubled, when the clavicle joint is integrated.

	Arm Range 7 DOF	Work-space 7 DOF	Arm Range 8 DOF	Work-space 8 DOF
to wrist	777 mm	1.9 m^3	1077 mm	3.4 m^3
to flange	924 mm	3.2 m^3	1224 mm	5.4 m^3
to TCP	1004 mm	4.2 m^3	1304 mm	6.6 m^3

TABLE III

RANGE AND WORKSPACE OF A SINGLE KIT ARM, SHOWING THE DIFFERENCE BETWEEN 7 DOF AND 8 DOF

D. Comparison with Other Robot Arms

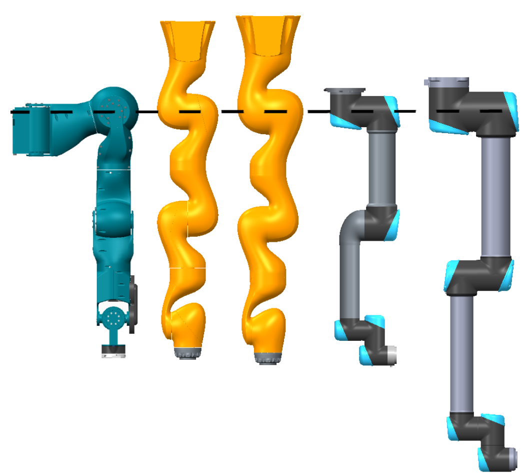

Fig. 4. Arm length comparison with the shoulder at the same height (from the left to the right: KIT Arm, KUKA LBR iiwa 7 R800, KUKA LBR iiwa 14 R820, UR5, UR10)

Table IV and Fig. 4 compare the KIT Arm with the industrial robot arms by UNIVERSAL ROBOTS [10] as well as the lightweight arms by KUKA [9], which are based on the DLR LWR III [14][15].

Fig. 4 illustrates the similarities between the KIT Arm and the KUKA/DLR lightweight arms in kinematics, when

TABLE IV
ARM COMPARISON

	Description	DLR LWR III	KUKA LBR iiwa 7 R800	KUKA LBR iiwa 14 R820	UR3	UR5	UR10	KIT Arm (single)
	Reference	[14][15]	[9]	[9]	[10]	[10]	[10]	
General	Payload	14 kg	7 kg	14 kg	3 kg	5 kg	10 kg	11 kg
	Weight	14 kg	23.9 kg	29.9 kg	11 kg	18.4 kg	28.9 kg	25 kg
	Payload-to-weight	1.00	0.29	0.47	0.27	0.27	0.35	0.44
	Arm range (to last joint)		800 mm	820 mm	500 mm	850 mm	1300 mm	1077 mm
	Arm range (to flange)	936 mm	926 mm	946 mm				1224 mm
	Workspace (to last joint)		1.7 m^3	1.8 m^3	0.5 m^3	3.2 m^3	9.2 m^3	3.4 m^3
	Degrees of freedom	7	7	7	6	6	6	8
Peak torques	Cla1	n/a	n/a	n/a	n/a	n/a	n/a	176 Nm
	Sho1	200 Nm	176 Nm	320 Nm	56 Nm	150 Nm	330 Nm	176 Nm
	Sho2	200 Nm	176 Nm	320 Nm	56 Nm	150 Nm	330 Nm	176 Nm
	Sho3	100 Nm	110 Nm	176 Nm	n/a	n/a	n/a	100 Nm
	Elb1	100 Nm	110 Nm	176 Nm	28 Nm	150 Nm	150 Nm	100 Nm
	Elb2	100/1.6 Nm	110 Nm	110 Nm	12 Nm	28 Nm	56 Nm	100 Nm
	Wri1	40 Nm	40 Nm	40 Nm	12 Nm	28 Nm	56 Nm	34 Nm
	Wri2	40 Nm	40 Nm	40 Nm	12 Nm	28 Nm	56 Nm	34 Nm
Maximum speed	Cla1	n/a	n/a	n/a	n/a	n/a	n/a	79°/s
	Sho1	120°/s	98°/s	85°/s	180°/s	180°/s	120°/s	79°/s
	Sho2	120°/s	98°/s	85°/s	180°/s	180°/s	120°/s	79°/s
	Sho3	120°/s	100°/s	100°/s	n/a	n/a	n/a	132°/s
	Elb1	120°/s	130°/s	75°/s	180°/s	180°/s	180°/s	132°/s
	Elb2	120°/s	140°/s	130°/s	360°/s	180°/s	180°/s	132°/s
	Wri1	120°/s	180°/s	135°/s	360°/s	180°/s	180°/s	206°/s
	Wri2	120°/s	180°/s	135°/s	360°/s	180°/s	180°/s	206°/s
Joint limits	Cla1	n/a	n/a	n/a	n/a	n/a	n/a	±82°
	Sho1	±170°	±170°	±170°	±360°	±360°	±360°	±∞
	Sho2	±120°	±120°	±120°	±360°	±360°	±360°	-22°/+202°
	Sho3	±170°	±170°	±170°	n/a	n/a	n/a	±∞
	Elb1	±120°	±120°	±120°	±360°	±360°	±360°	-36°/+154°
	Elb2	±170°	±170°	±170°	±360°	±360°	±360°	±∞
	Wri1	-45°/+80°	±120°	±120°	±360°	±360°	±360°	±40°
	Wri2	-30°/+60°	±175°	±175°	±360°	±360°	±360°	±90°

the clavicle joint is not considered. They have spherical joints in the shoulder and wrist, a comparable maximum arm length from the shoulder to the flange and similar workspace volumes (compare also Table III with Table IV). While the KUKA LBR arms have a bigger freedom of movement in their wrist, the KIT Arm allows continuous rotation for *Sho1*, *Sho3* and *Elb2*. When the influence of the clavicle joint is taken into account, the KIT Arm surpasses all other robot arms of Table IV in range and workspace, except from UR10. As with all robot arms of the UR-series, the joint limits of UR10 are ±360°. This results in a spherical workspace with as radius of 1.3 m. However, this joint freedom is realized through non-human-like displacements in the shoulder, elbow and wrist joints. Furthermore, the joint for the rotation of the upper arm is missing. Therefore, the UR robots have neither a spherical joint in the shoulder nor a spherical joint in the wrist. They have only 6 DOF and no redundancy: There is only one joint configuration for each oriented TCP pose.

Considering the peak torques of the shoulder, the KIT Arm (176 Nm) is comparable to the DLR LWR III (200 Nm), KUKA LBR iiwa 7 R800 (176 Nm) and UR5 (150 Nm). The UR10 and KUKA LBR iiwa 14 R820 have significantly higher peak torques in the shoulder joints (330 Nm and 320 Nm). However, the maximum payload is almost comparable: While UR 10 can hold 10 kg and the KUKA LBR iiwa 14 R820 is able to hold 14 kg, the KIT Arm can handle payloads of up to 11 kg at long range. This can be explained by the lightweight design of the KIT Arm, using a hollow structure and a preferably short distance between the shoulder and the relatively heavy sensor-actuator-control units, especially in the wrist (see Section III). The KIT Arm has a total weight of approx. 25 kg. Without the clavicle joint, the weight is reduced to approx. 20 kg and therefore approx. 9-10 kg less than the weight of UR10 (28.9 kg) and KUKA LBR iiwa 14 R820 (29.9 kg). As depicted in Fig. 4 the distance between the shoulder and wrist of all shown robots is comparable, except for UR10, which has a distance that is approx. 500 mm longer. This results in higher peak torques for the same payload. In contrast, the addition of the clavicle joint and the gained reach do not influence the payload of the KIT Arm at all. As we consider that the arms are installed in a vertical basis position with a maximum angle variation of +/-45° (e.g. through a hip construction of a humanoid robot), the clavicle joint (*Cla1*) does not need to have a higher peak torque than the shoulder joints (*Sho1,2*), although the maximum range is longer. The higher weight by the integration of the clavicle joint reduces the payload-to-weight-ratio from 0.55 to 0.44, which is still high compared to most of the other arms in the table. The only exception is the DLR LWR III, which uses a carbon fibre composite structure instead of aluminum (alloys) in contrast to the other arms, which are presented in Table IV. Although carbon fiber composite has better characteristics for lightweight arms, we decide in favor of a structure based on high-strength aluminum, which allows a higher design freedom and a less complicate manufacturing process.

III. REALIZATION OF THE ARM DESIGN

A. Sensor-Actuator-Control Units

The mechanical design of the arm is built around a set of modular *sensor-actuator-control units*, with each joint comprising one of those units. Well-defined, minimal mechanical and electrical interfaces make these drive units easy to integrate and thus allow a slim overall robot design. Modularity facilitates the usage of the same drive units in different joints of the presented robot, as well as in future projects.

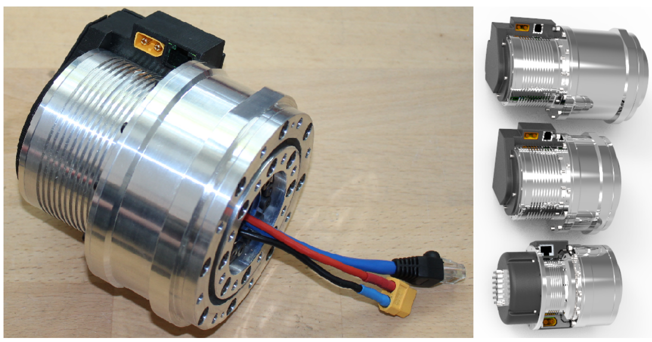

Fig. 5. Left: Functional prototype of the mid-size sensor-actuator-control unit. Note the DC and EtherCAT connections on the left (upstream) and on the right, at the center of the output flange (downstream). Right: Rendering of the sensor-actuator-control unit in three sizes

The design of the sensor-actuator-control units is based on the integrated drive units of the humanoid robot ARMAR-4 [4]. There, each joint in the arms, legs and torso is equipped with a sensor-actuator unit that includes the motor and gear as well as position, temperature and torque sensors. However, the electronics that control the motor and the sensors are located externally, necessitating a set of cables between them and the sensor-actuator units. Handling the external cables and preventing damage to them has proven to be a substantial challenge, which is why we seek to avoid them in the presented design.
To this end, the developed sensor-actuator control units include the motor, sensors and all necessary electronic components for controlling the motor and interfacing the sensors in a single, encapsulated housing. The only external interfaces are to the DC-bus for power supply, and to the EtherCAT bus for communication. Those connections are fed through the drive unit via a slip ring that enables continuous rotation without putting any stress on the internal wires. This feature also allows effortless chaining of actuators. The core components of each drive unit are a brushless DC motor, a Harmonic Drive unit, incremental and absolute position encoders, a 9-axis inertial measurement unit, an output torque sensor, a motor temperature sensor, a microcontroller that links the sensors to the EtherCAT bus, and a highly efficient motor controller to minimize heat production.
The drive train is back-drivable, resulting in a system that is inherently 'safe-by-design'. The torque-sensing capability and high bandwidth of the EtherCAT bus furthermore allow the implementation of a high-speed active impedance control system for safe interaction.
To meet the different requirements in the different arm joint locations, we developed a family of sensor-actuator-control units comprising three different sizes with maximum torques of 176 Nm, 123 Nm and 64 Nm (see Fig. 5). All units have in common the set of core components described above.

B. Arm Structure

For the arm structure, we investigate two alternatives, which both allow the integration of sensor-actuator-control units: A structure based on an exoskeleton approach and a structure based on a classic frame construction (see Fig. 6).

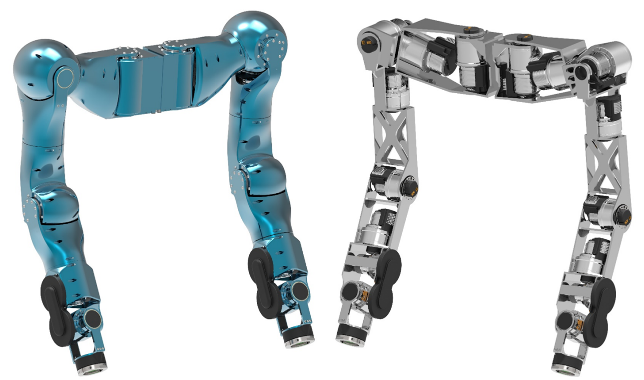

Fig. 6. Two different structure designs (left: exoskeleton approach (rendering), right: frame construction (rendering))

A classic frame construction, as it was used for ARMAR-III [3] and ARMAR-4 [4], is an easy way to link the modular sensor-actuator-control units mechanically. The numerous but simple parts can be manufactured easily with a modest milling machine at low cost. Linked through screw connections, many parts are building a lightweight frame structure. This also results in a high adaptability, which is useful for prototype design. If needed, a covering can be added by attaching it to the frame parts.

In contrast, the exoskeleton design approach is based on a hollow structure that is load-bearing structure and covering at the same time. Thereby, it is based on only few complex parts. The advances in manufacturing processes during the last years, allow a great design freedom. Modern casting processes, 5-axis milling machines and the booming additive manufacturing sector make it possible to realize complex 3D lightweight constructions. Structures based on pipe cross-sections are a good match for the various load types a robot arm has to endure. An optimized hollow structure with a good flux of force increases the stiffness and therefore the precision of the arm at a low weight. In addition, the exoskeleton design approach allows an easy covering of the cables that increases the robustness of the robot as well as the safety for humans working with the robot. Examples for robots using the exoskeleton design approach are WALK-MAN [7] and the DLR/KUKA lightweight robot arms [9][14][15].

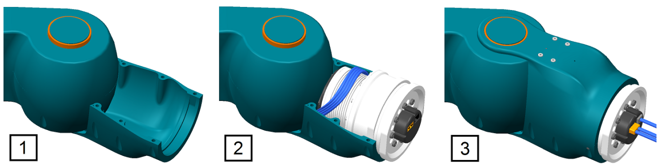

Fig. 7. Integration of a sensor-actuator-control-unit into the hollow structure

As there are many advantages as robustness, safety, precision and maintainability, which are crucial for a robot arm that is supposed to be used in a realistic (non-laboratory) environment, we choose the exoskeleton approach. As shown in Fig. 7, the modular sensor-actuator-control units and the cables between those units are fully covered by a hollow structure which is the load-bearing structure at the same time. The units can be easily integrated: Mechanically, the casing and the output are linked to the structure either via a screw flange or a clamped ring. Electronically, the daisy-chained units are linked via connectors. This allows for convenient maintenance: If a unit is damaged, it can be exchanged quickly.

C. Wrist Design

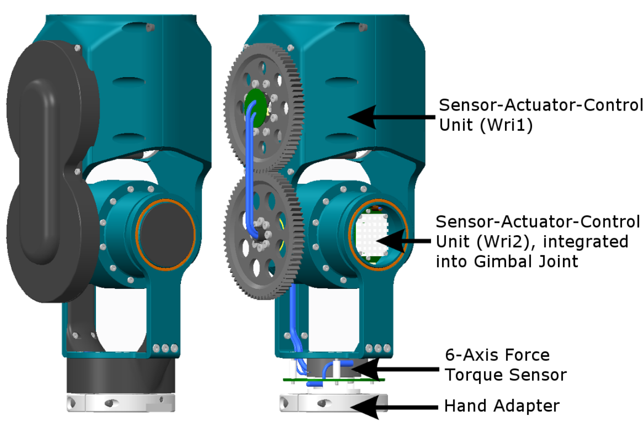

Fig. 8. Wrist mechanism (left: covered, right: uncovered)

As described in the kinematic model of Section II, the KIT Arm has a spherical joint in its wrist. Whereas the first joint's sensor-actuator-control unit is placed in the forearm next to the elbow (*Elb2*), the last two wrist joints (*Wri1,2*) are realized in the form of a gimbal joint. Since an anthropomorphic wrist is limited in space, the gimbal joint's cross includes only one sensor-actuator-control unit (*Wri2*). The other unit is located parallel to the axis (*Wri1*). The transmission is realized through lightweight optimized gears at the unit's output flange. Although this necessitates gears with a big diameter, this solution allows the consequent realization of the modular approach, including an easy integration and maintainability.

Fig. 8 shows on the left side the wrist with all covers. 3D printed parts (black) are covering the cables and protecting them from contact with the gears. On the right side, the covering parts are hidden and therefore the cabling (blue) is visible: Passing through holes in the gears, the cables enter into the gimbal joint and lead down to the hand adapter, which is equipped with a 6-axis force torque sensor. The hand adapter offers a well-defined electronic and mechanical interface. Thus, the end effector can be easily exchanged.

D. Static Analysis

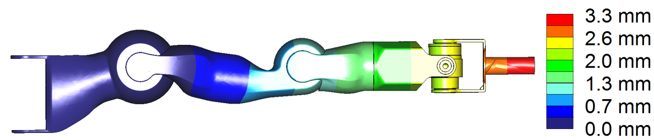

Fig. 9. Static analysis: Displacement at full load (11 kg)

As part of the design phase, we conduct a static analysis for every part of the arm structure to ensure a safety factor $S = 2$ against plastic deformation. Furthermore, the deflection of the whole arm at long range is analyzed and thereby the displacement of the TCP. At full load (11 kg), the displacement of the TCP caused by the elasticity of the arm structure is approx. 3.3 mm (Fig. 9), whereas without load except from the arm's own weight, it is approx. 1.1 mm. Taking into account the elasticity in the bearings, the total displacement is approx. 5.2 mm at full load and 2.5 mm at no load. The displacement is largely reduced through rigid cross roller bearings and the double-sided mounting of the arm structure of joint *Cla1, Sho2, Elb1, Wri1* and *Wri2*.

IV. REACHABILITY ANALYSIS

A. Single Arm Manipulation

Fig. 10 (left) shows the results of our studies on the reachability of a single KIT Arm. As presented in [20], the reachability of a Cartesian voxel corresponds to the volume in configuration space that results in a TCP pose within the voxel. The warmer the color of the volume unit the more configurations are possible. In contrast, the manipulability as described by Yoshikawa [21] is best in the center of the workspace (see Fig. 10 (right)).

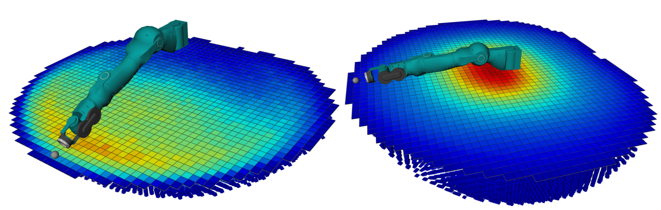

Fig. 10. Reachability (left) and manipulability (right) analysis of a single KIT Arm (sectional view). The warmer the color, the higher the value.

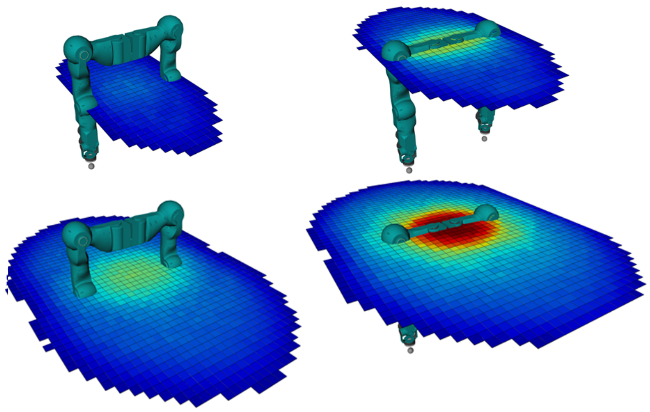

Fig. 11. Bimanual manipulability (sections): Comparison of a 14 DOF version (top row) with the 16 DOF KIT Dual Arm System (bottom row)

B. Dual Arm Manipulation

Due to the symmetrical workspace and joints with continuous rotation, the dual arm system consists of two identical KIT Arms. Since the arms have modular interfaces, the distance between the arms can be chosen freely. As standard configuration, we chose a distance of 180 mm between the clavicle joints of the right and the left arm. This results in a total workspace of $8.4\,\mathrm{m}^3$ for the $2{\times}8{=}16$ DOF bimanual system and $6.5\,\mathrm{m}^3$ for the $2{\times}7{=}14$ DOF system, in which the clavicle joint is fixed for each arm.

We evaluate the manipulability of the 16 DOF bimanual system and compare the results to the 14 DOF system. Therefore, we investigate for each volume unit if it can be reached by both end-effectors. If so, the bimanual manipulability at this point is derived by computing the average of the two single-arm manipulability values. As depicted in Fig. 11, the bimanual workspace of the 14 DOF version ($1.8\,\mathrm{m}^3$, see top row) is smaller compared to the 16 DOF system ($4.9\,\mathrm{m}^3$, see bottom row). In addition, the achieved manipulability values are lower, which indicates that making use of the clavicle joint results in higher dexterity and maneuverability for bimanual tasks.

V. CONCLUSION AND FUTURE WORK

In this paper we presented the KIT Dual Arm System, which consists of two high-performance humanoid robot arms. In addition to a description of its humanoid kinematics, we compared its characteristic data to state-of-the-art robot arms. We discussed the arm structure, which is based on an exoskeleton design approach that includes highly integrated modular sensor-actuator-control units. The focus of this paper was on the integration of an additional joint: a clavicle joint of the human inner shoulder. We analyzed and demonstrated the positive influence of this clavicle joint on the arm range, workspace and the manipulability, especially for dual arm manipulation. Combining the advantages of human kinematics with the high performance and stiffness of industrial robots, we presented a dual arm system which is designed for human-robot interaction in different environments.

Future work will include further analysis as well as practical experience as soon as the assembly of the arms is finished. Furthermore, we will integrate the KIT Dual Arm System into a humanoid robot for mobile dual arm manipulation in non-laboratory environments.

REFERENCES

[1] K. Kaneko, F. Kanehiro, S. Kajita, H. Hirukawa, T. Kawasaki, M. Hirata, K. Akachi, and T. Isozumi, "Humanoid robot HRP-2," in *IEEE Int. Conf. on Robotics and Automation (ICRA)*, vol. 2, 2004, pp. 1083–1090.

[2] K. Kaneko, F. Kanehiro, M. Morisawa, K. Miura, S. Nakaoka, and S. Kajita, "Cybernetic human HRP-4C," in *IEEE/RAS Int. Conf. on Humanoid Robots (Humanoids)*, 2009, pp. 7–14.

[3] T. Asfour, K. Regenstein, P. Azad, J. Schröder, A. Bierbaum, N. Vahrenkamp, and R. Dillmann, "ARMAR-III: An integrated humanoid platform for sensory-motor control," in *IEEE/RAS Int. Conf. on Humanoid Robots (Humanoids)*, 2006, pp. 169–175.

[4] T. Asfour, J. Schill, H. Peters, C. Klas, J. Bücker, C. Sander, S. Schulz, A. Kargov, T. Werner, and V. Bartenbach, "ARMAR-4: A 63 DOF Torque Controlled Humanoid Robot," in *IEEE/RAS Int. Conf. on Humanoid Robots (Humanoids)*, 2013, pp. 390–396.

[5] "Boston Dynamics". Atlas. Anthropomorphic Robot. [Online]. Available: http://archive.darpa.mil/roboticschallengetrialsarchive/files/ATLAS-Datasheet_v15_DARPA.pdf

[6] S. Kagami, N. Nishiwaki, J. J. Kuffner Jr., T. Sugihara, M. Inaba, and H. Inoue, "Design, Implementation, and Remote Operation of the Humanoid H6," *Experimental Robotics VII Lecture Notes in Control and Information Sciences*, vol. 271, pp. 41–50, 2001.

[7] M. Bagheri, A. Ajoudani, J. Lee, D. G. Caldwell, and N. G. Tsagarakis, "Kinematic Analysis and Design Considerations for Optimal Base Frame Arrangement of Humanoid Shoulders," in *IEEE Int. Conf. on Robotics and Automation (ICRA)*, 2015, pp. 2710–2715.

[8] M. Okada and Y. Nakamura, "Development of a Cybernetic Shoulder," *IEEE Trans. on Robotics*, vol. 21, no. 3, pp. 438–443, 2005.

[9] "KUKA Robot GmbH". [Online]. Available: http://www.kuka.com

[10] "Universal Robots". [Online]. Available: http://www.universal-robots.com

[11] "ABB". YuMi creating an automated future together. You and Me (Data Sheet). [Online]. Available: http://new.abb.com/products/robotics/yumi

[12] "Rethink Robotics". Baxter Datasheet. [Online]. Available: http://www.rethinkrobotics.com/baxter

[13] "YASKAWA". Motoman SDA-series. Flexible Applications with the SDA-series. [Online]. Available: http://www.yaskawa.eu.com

[14] A. Albu-Schäffer, S. Haddadin, C. Ott, A. Stemmer, T. Wimböck, and G. Hirzinger, "The DLR lightweight robot - Design and Control Concepts for Robots in Human Environments," *Industrial Robot: An International Journal*, vol. 34, no. 5, pp. 376–385, 2007.

[15] "DLR Robotics and Mechatronics Center". DLR Light-weight Robot III. [Online]. Available: http://www.dlr.de

[16] C. Ott, O. Eiberger, W. Friedl, B. Bäuml, U. Hillenbrand, C. Borst, A. Albu-Schäffer, B. Brunner, H. Hirschmüller, S. Kielhöfer, R. Konietschke, M. Suppa, T. Wimböck, F. Zacharias, and G. Hirzinger, "A humanoid two-arm system for dexterous manipulation," in *IEEE/RAS Int. Conf. on Humanoid Robots (Humanoids)*, 2006, pp. 276–283.

[17] "FRANKA EMIKA". [Online]. Available: https://www.franka.de

[18] T. Asfour, *Sensomotorische Bewegungskoordination zur Handlungsausführung eines humanoiden Roboters*. Ph.D. thesis, Department of Informatics, University of Karlsruhe, 2003.

[19] "ISO International Organization for Standardization", "ISO 3411. Earth-moving machinery - Physical dimensions of operators and minimum operator space envelope (ISO 3411:2007)."

[20] N. Vahrenkamp, T. Asfour, and R. Dillmann, "Efficient Inverse Kinematics Computation based on Reachability Analysis," *International Journal of Humanoid Robotics*, vol. 9, no. 4, pp. 0–0, 2012.

[21] T. Yoshikawa, "Manipulability of Robotic Mechanisms," *The International Journal of Robotics Research*, vol. 4, no. 2, pp. 3–9, 1985.